Distribution of Muscarinic Acetylcholine Receptors and Presynaptic Nerve Terminals in Amphibian Heart

H. CRISS HARTZELL with the technical assistance of Jan Zwemer
Department of Anatomy, Emory University School of Medicine, Atlanta, Georgia 30322

ABSTRACT At many synapses, neurotransmitter receptor molecules in the postsynaptic membrane are selectively concentrated at a site directly opposite the presynaptic nerve terminal. In this paper, I examine acetylcholine (ACh) receptor distribution in cardiac muscle in relation to the distribution of presynaptic axonal varicosities. The density of varicosities, stained with zinc iodide and osmium, ranges from 0.7/100 μm^2 in ventricle to 1.9/100 μm^2 in sinus venosus. It is estimated that <3% of the muscle surface is apposed to presynaptic varicosities. ACh receptors, however, are randomly distributed on the muscle surface and not concentrated in patches. ACh receptor distribution was determined by iontophoretic application of ACh and mapping of ACh sensitivity and by [^{3}H]QNB (quinuclidinyl benzilate) binding and autoradiography. [^{3}H]QNB binds with >90% specificity to a single, saturable, high-affinity (K_d = 11.1 pM at 21°C) class of binding sites. QNB binding sites are thought to correspond to ACh receptors, because muscarinic agonists compete for [^{3}H]QNB binding and produce a hyperpolarization in the sinus venosus with the same order of potency. The concentrations of QNB binding sites in the sinus and atria are about twice those found in ventricle. The receptor density corresponds to the density of innervation measured by zinc iodide and osmium staining. Autoradiographic experiments show that [^{3}H]QNB binding sites are distributed randomly over the entire surface of the muscle. This random distribution of ACh receptors in cardiac muscle has important implications for the function of the cardiac neuroeffector junction.

Parasympathetic inhibition of the heart is mediated by the interaction of acetylcholine (ACh) with muscarinic acetylcholine receptors (mAChR) on the surface of cardiac muscle cells. This interaction produces a decrease in the force and rate of contraction (3, 38). Current evidence suggests that the slowing of the rate is mediated by a increase in the potassium conductance of the membrane (and a hyperpolarization), whereas the decreased force of contraction is the result of a decreased influx of calcium during the action potential (13, 15, 31, 53).

The cardiac neuroeffector junction has several interesting features that are not completely understood. The autonomic axons in the heart are composed of long chains of varicosities that seldom come into close contact (<50 nm) with the cardiac muscle cells. Further, morphological specialization of the postsynaptic membrane is rarely seen (reviewed in reference 17). These features suggest that there is little, if any, differentiation between junctional and nonjunctional membrane in cardiac muscle cells. This is in contrast to the skeletal neuromuscular junction and many interneuronal synapses in which pre- and postsynaptic membranes are closely apposed and the postsynaptic membrane is morphologically specialized. A common feature of such morphologically specialized postsynaptic membranes is the localization of neurotransmitter receptor molecules to the region of membrane directly subjacent to presynaptic transmitter release sites (9, 10, 19, 33, 40, 51). The purpose of the present study was to determine whether a similar patchy distribution of ACh receptors could be detected in cardiac muscle cells. These studies show that ACh sensitivity and mAChR are widely distributed over the entire surface of the cardiac muscle membrane and that ACh released from the autonomic axons has a diffuse effect on the cardiac muscle. A preliminary note has appeared (21).

MATERIALS AND METHODS

Preparation

Experiments were performed on hearts of *Xenopus laevis* and *Rana pipiens* in both summer and winter. No consistent differences were observed between *Rana* and *Xenopus* or between summer and winter frogs. Differences in the concentration of 3-quinuclidinyl benzilate (QNB) binding sites have been observed, however, between batches of frogs. For anatomical and electrophysiological experiments, heart tissue was pinned onto a coverslip coated with a thin layer of cured Sylgard (Dow Corning Corp., Midland, Mich.) resin. Normal Ringer

THE JOURNAL OF CELL BIOLOGY · VOLUME 86 JULY 1980 6–20

solution contained 111 mM NaCl, 2 mM KCl, 2 mM $CaCl_2$, and 1 mM Na-HEPES buffer, pH 6.8. For physiological experiments, Ringer solution was used in which 1 μg/ml D600 or 4 mM $MnCl_2$ was added (NaCl was reduced 6 mM to maintain osmolarity when Mn^{+2} was added) to eliminate spontaneous beating.

Electrical Recording and Iontophoresis

Standard electrophysiological recording and iontophoretic techniques were used as previously described (21–23). Recording microelectrodes were fabricated from fiber-filled capillaries, were backfilled with 3 M KCl, and had resistances of 60–120 MΩ. Iontophoretic pipets were pulled similarly but filled with 2 M ACh-Cl. Braking currents of 4–8 nA were placed on the iontophoretic pipets to prevent outward diffusion of ACh. Because heart muscle ACh receptors do not noticeably desensitize during ACh application (16), elaborate precautions for adjusting braking current were not necessary (24). Iontophoretic doses of ACh are expressed as nanocoulombs (nC) of charge passed through the iontophoretic pipet. Chemosensitivity is expressed as peak hyperpolarization (in millivolts) produced by ACh (in nanocoulombs). In some experiments the time integral of the response was measured by tracing photographs of responses on a 9864A Digitizer (Hewlett-Packard Co., Palo Alto, Calif.) and calculating the areas with an HP 9810 calculator. Recording and iontophoretic pipets were positioned under visual control using Nomarski differential interference contrast optics at a magnification of ×500, using a water immersion objective with a working distance of 1.6 mm (39). Solutions were applied to the bath by changing the perfusion reservior. Perfusion rate was ~1 ml/min. Several minutes were required for the new solution to enter and exchange the bath.

Zinc Iodide and Osmium

Axonal varicostities were stained with zinc iodide and osmium tetroxide (ZIO) (2, 37, 46). A zinc iodide solution was made by mixing 2 g of Zn dust and 1 g of I_2 in 40 ml of H_2O. 2 ml of the filtered zinc iodide, 0.5 ml of 2% aqueous OsO_4, and 6 ml of 0.2 M sodium acetate buffer, pH 3.9, were mixed to make the buffered ZIO solution. Fresh frog muscle was immersed in buffered zinc iodide and osmium solution overnight at 4°C. After incubation in ZIO, the preparation was rinsed in H_2O, dehydrated rapidly in graded ethanol series, cleared with xylene, and mounted on a glass microscope slide in Protexx mounting medium (Scientific Products, Atlanta, Ga.). ZIO stains both cholinergic and aminergic nerve terminals (see references 2 and 46).

Electron Microscopy

Freshly dissected frog muscle was fixed in 1% glutaraldehyde buffered with sodium phosphate, pH 7.2, (250 mOsm) and postfixed in phosphate-buffered 1% OsO_4 (39). Fixed material was dehydrated in ethanol and embedded in Epon 812 resin. Silver sections were examined on a Philips 400 electron microscope.

QNB Binding

Binding of QNB to homogenates of frog muscle was performed as described by Yamamura and Snyder (59) and Fields et al. (11). Briefly, hearts were homogenized in a Teflon-pestle, glass-tube homogenizer in 50 mM sodium-phosphate buffer, pH 7.4, at 4°C. Aliquots of the homogenates containing 0.01–0.5 mg of protein and 5–80 fmol of QNB binding sites were added to tubes containing 2 ml of 50 mM sodium-phosphate buffer, pH 7.4, [^{3}H]QNB, and other additions as noted. Bound [^{3}H]QNB was separated from free [^{3}H]QNB by vacuum filtration through GF/C glass-fiber filters (Whatman, Inc., Clifton, N. J.). The filters were washed four times with 5 ml of ice-cold phosphate buffer, air-dried, and placed in Triton-toluene scintillation fluid (1 liter of Triton X-100, 2 liter of toluene, 12.7 g of PPO (2,5-diphenyloxazole), and 0.3 g of POPOP (*p*-bis[2-(5-phenyloxazolyl)]benzene)). Samples were counted at an efficiency of 40% in an LS230 liquid scintillation counter (Beckman Instruments, Inc., Fullerton, Calif.). Each filter contained 100–900 cpm of specific [^{3}H]QNB binding. The [^{3}H]QNB was a mixture of active (−) and inactive (+) isomers. It was assumed that the ratio of (+) and (−) isomers was 1.0 in calculating (−) [^{3}H]QNB concentrations. Free (−) [^{3}H]QNB concentration was calculated as the difference between total and bound (−) [^{3}H]QNB. Adsorption of QNB to glassware was negligible. Experimental points were usually determined in triplicate. Several batches of [^{3}H]QNB were used (New England Nuclear, Boston, Mass.; [4,4′-^{3}H]QNB, 29.4 Ci/mmol; Amersham Corp., Arlington Heights, Ill.: [3-^{3}H]QNB, 16.4 Ci/mmol). Unlabeled QNB was a gift from Hoffmann-La Roche, Inc., Nutley, N. J.

Analysis of QNB-Receptor Interaction

Experiments were performed to analyze the equilibrium dissociation constant (K_d) and on- and off-rates of QNB binding to its receptor. The equilibrium K_d was determined by measuring bound [^{3}H]QNB as a function of the concentration of free [^{3}H]QNB at equilibrium. The time required to reach equilibrium was determined in separate experiments (below). The K_d was determined from the slope of Scatchard (52) plots, assuming the following model for ligand-receptor interaction. (See reference 30 for valuable discussion of receptor binding analysis.) The reversible interaction of $[L]$ with receptor $[R]$ to form a ligand-receptor complex $[LR]$ is described by the relation:

$$L + R \underset{k_{off}}{\overset{k_{on}}{\longleftrightarrow}} LR. \tag{1}$$

The equilibrium dissociation constant, K_d, is given by:

$$K_d = \frac{[R]_e[L]_e}{[LR]_e}, \tag{2}$$

where subscript e denotes equilibrium concentrations. Rearrangement and linearization according to the method of Scatchard gives the relationship:

$$[LR]_e = \frac{[LR]_e}{[L]_T}(-K_d) + [R]_T, \tag{3}$$

where T indicates total concentration. The Scatchard plot of the ratio of bound to free ligand ($[LR]_e/[L]_e$) vs. bound ligand ($[LR]_e$) then gives a straight line with a slope of $-1/K_d$ and an x-intercept of $[R]_T$.

The rate of QNB binding to the high affinity site was determined by measuring [^{3}H]QNB binding as a function of time at different [^{3}H]QNB concentrations. Homogenates were added to [^{3}H]QNB solutions at t = 0, incubated for a predetermined time, and rapidly filtered. Filtration terminated the reaction within 10–20 s. If QNB binding is a bimolecular process according to Eq. 1 the rate of formation of $[LR]$ is given by the differential rate equation:

$$\frac{d[LR]}{dt} = k_{on}[L][R] - k_{off}[LR]. \tag{4}$$

Integration gives:

$$\ln\left(\frac{[LR]_e}{[LR]_e - [LR]_t}\right) = (k_{on}[L]_T + k_{off})\cdot t. \tag{5}$$

The k_{off} was determined by examining the decrease in previously bound [^{3}H]QNB after addition of competitor (50 nM unlabeled QNB or 100 μM oxotremorine) as a function of time. The k_{off} was calculated from the equation:

$$k_{off} = \frac{1}{t}\cdot \ln\left(\frac{[LR]_e}{[LR]_t}\right), \tag{6}$$

where $[LR]_e$ is concentration of bound ligand immediately before addition of competitor.

The ability of various muscarinic agonists and antagonists to compete for QNB binding was determined by addition of these competitors to a standard incubation mixture containing 0.5 nM (±) [^{3}H]QNB. The incubation was started by addition of homogenate and carried out for 90 min. The Hill coefficient (6) was evaluated from the equation:

$$\log\left(\frac{[LR]_e}{[R]_T - [LR]_e}\right) = n \log (I), \tag{7}$$

where (I) is inhibitor concentration.

Autoradiography

Distribution of QNB binding sites was determined by autoradiography of muscle fibers labeled with [^{3}H]QNB. Pieces of *Xenopus laevis* interatrial septum or sinus venosus were incubated in [^{3}H]QNB in Ringer solution for 1–4 h at 21°C, washed with many changes of ice-cold Ringer solution for 2 h, and fixed for 30 min in 1% glutaraldehyde buffered with sodium phosphate, pH 7.2. Most preparations were subsequently washed in Ringer's an additional 2–10 h at 4°C. The thinnest portions of the preparations were cut out and placed on a 1-cm-diameter round coverslip with a drop of 1% bovine serum albumin and quickly dried under a stream of air at 4°C. A thin layer of carbon was then evaporated onto the preparation. The slide was coated with emulsion by a method similar to that of Lane et al. (34). Glass microscope slides were dipped in a solution of 2% celloidin in amyl acetate and dried. The celloidin-coated slide was then dipped in melted Kodak NTB-2 emulsion (diluted 1:1 with distilled water) and air-dried. The emulsion-celloidin film was floated off the microscope slide onto a water bath at room temperature using a Wratten no. 2 filter (Eastman Kodak Co., Rochester, N. Y.) for illumination. The coverslip with the preparation was placed on the floating emulsion so that the preparation made firm contact with the

emulsion layer. The coverslip and attached celloidin-emulsion layer was picked up by suction onto a filter paper support. A square of filter paper was placed on the filter-supporting surface of a Swinnex 45-mm filter holder (Millipore Corp., Bedford, Mass.) attached to a vacuum line. The filter paper and holder were then advanced slowly toward the floating coverslip until the vacuum sucked the coverslip and emulsion onto the filter paper. By this method, it was possible to cover the preparation with emulsion without its getting wet. The emulsion was exposed at 4°C in a dessicator for 10–14 d. The celloidin film was removed with several washes of absolute ethanol. The autoradiograph was developed at 15°C in Kodak Dektol developer for 2 min, rinsed in dH_2O, and fixed in Kodak fixer for 5 min. Nonspecific binding was measured in preparations that had been incubated in [^{3}H]QNB and 100 nM unlabeled (±) QNB or 100 μM atropine.

RESULTS

Experiments were performed on the frog heart. Although all regions of the heart were examined, electrophysiological and anatomical studies focused upon the sinus venosus, which is the primary pacemaker region, and the interatrial septum. The preparations are very thin sheets of tissue often not more than 20-μm thick and are well suited for iontophoretic mapping experiments, because they can be viewed with Nomarski optics, and for anatomical studies using whole mounts.

Anatomy of the Preparation

In living preparations viewed with Nomarski optics, one can see considerable cellular detail. In both the sinus and the interatrial septum, electrically coupled muscle cells are organized into bundles that run through the preparation (Fig. 1 *a*).

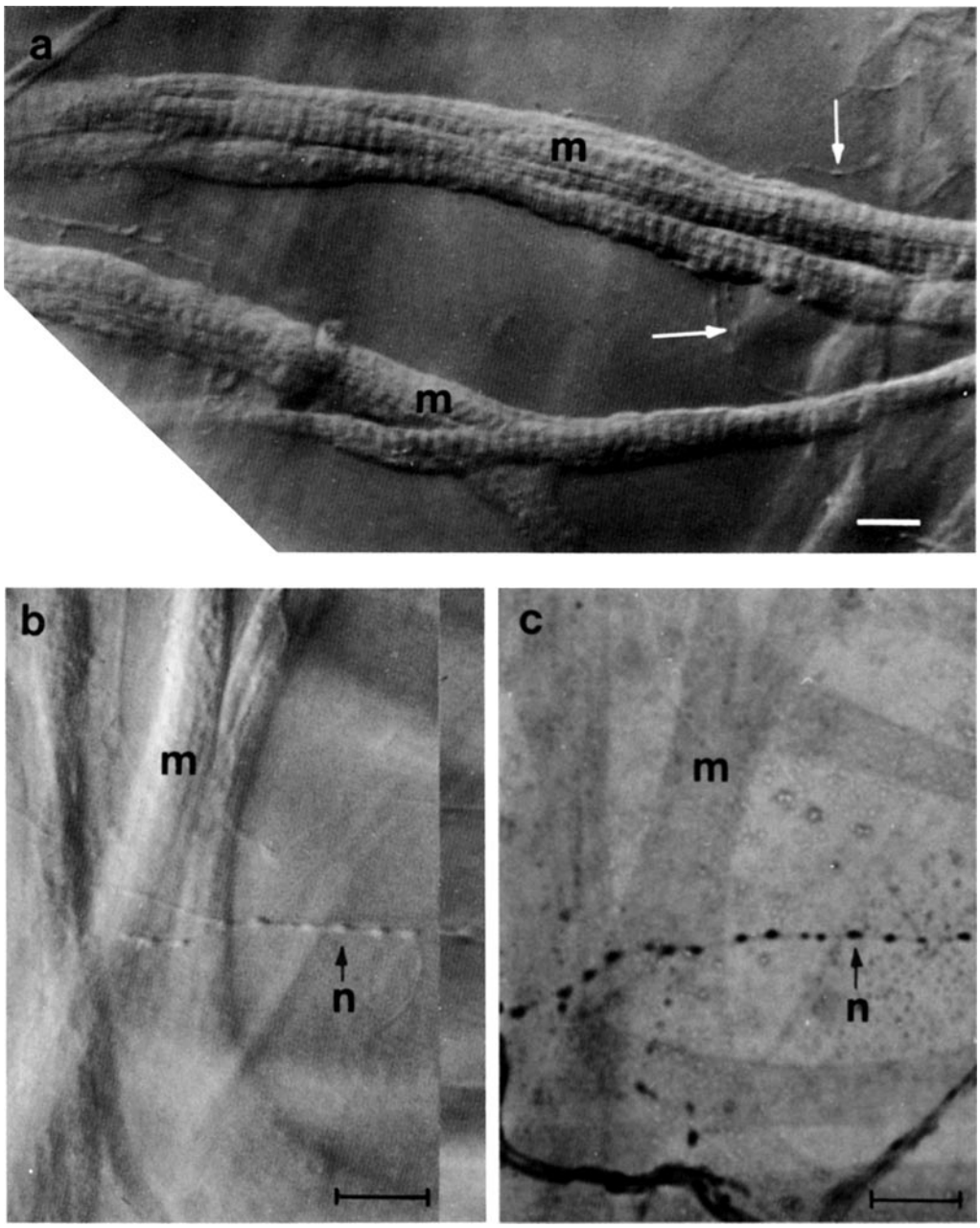

FIGURE 1 Muscle fibers and axonal varicosities in *Xenopus* heart. *(a)* Nomarski differential interference contrast micrograph of a small group of muscle fibers (*m*) in the living sinus venosus. Arrows point to segments of varicose axons innervating these fibers. *(b)* Portion of interatrial septum viewed with Nomarski optics. A chain of varicosities (arrow, *n*) enters the field at the right and crosses ~50 μm devoid of muscle fibers before it contacts the muscle fiber (*m*) at the left. *(c)* Same field as in *b* after staining with zinc iodide and osmium. Arrows in *b* and *c* indicate the same varicosity. Bars, 10 μm.

The muscle "fibers" range from 3 to 50 μm in diameter and branch extensively. In favorable preparations it is possible to see the terminal branches of the varicose autonomic axons that innervate these cells. In Fig. 1 *a* and *b*, varicose axons (arrows) can be seen most clearly where they traverse areas devoid of muscle fibers. Occasionally, the axons extend across the surface of the muscle fibers (Fig. 1 *b*). Varicosities on the muscle surface, however, are usually difficult to resolve with Nomarski optics.

The distribution of varicosities can be studied more easily in preparations that have been fixed and stained with ZIO (Figs. 1 *c* and 2). Fig. 1 *c* shows the same field seen in Fig. 1 *b* after staining with ZIO. In this particular field, almost all of the ZIO-stained varicosities can also be seen in the Nomarski view (Fig. 1 *b*). This particular region, however, was sparsely innervated. A more densely innervated area is seen in Fig. 2. In Fig. 2, varicosities are very densely distributed on the surface of the muscle fibers and are also found in the spaces between muscle fibers. To estimate the average area of muscle surface apposed to varicosities, the average cross-sectional area of varicosities and the density of varicosities on the muscle surface were measured from micrographs of ZIO-stained preparations. ZIO-stained varicosities do not noticeably differ in size from living varicosities (compare Fig. 1 *b* with Fig. 1 *c*). ZIO-stained varicosities measure 1.05 ± 0.45 μm in the short dimension by 1.44 ± 0.48 μm in the long dimension (mean ± standard deviation, $n = 70$). Thus, an average varicosity has a cross-sectional area of 1.2 μm^2. The density of varicosities on muscle fibers varies in different regions of the heart. The average density was 1.9 varicosities/100 μm^2 in the sinus venosus, 1.6 varicosities/100 μm^2 in the atrium and interatrial septum, and 0.7 varicosity/100 μm^2 in the ventricle. From the varicosity density and average varicosity cross-sectional area, it is calculated that the average area of muscle apposed to varicosities ranges from 2.2% in sinus venosus to 0.8% in ventricle. Because some of the varicosities that were counted were located several micrometers from the muscle, however, it seems likely that the actual focal synaptic area is less than the above estimate.

Varicosities are presumptive sites of transmitter release. Electron micrographs (Fig. 3) demonstrate that varicosities are packed with synaptic vesicles, even when they are located several micrometers from the muscle. A quantitative analysis of the frequency of close synaptic contacts was not made. However, in numerous electron micrographs most of the varicosities were located >50 nm away from the nearest muscle cell.

Chemosensitivity of the Postsynaptic Membrane

The chemosensitivity of the cardiac muscle membrane was measured by recording the hyperpolarization produced by iontophoretic application of acetylcholine. The spontaneous beating of the preparation was arrested by placing the preparation in Ringer solution containing 4 mM $MnCl_2$. Fine-tipped, ACh-containing, iontophoretic pipets (>100 MΩ resistance) were positioned onto an impaled muscle fiber viewed with Nomarski optics as described previously (20).

Fig. 4 *a* illustrates the responses of a fiber to 5-ms-duration pulses of ACh delivered from a micropipet. Responses rise to a peak in 1–2 s and have half-decay times (shown by open circles) of 2–3 s. Responses to iontophoretic ACh are about two times slower than those produced by stimulation of the vagus nerve (Fig. 4 *b*). Times to peak and half-decay times for pipet-evoked responses increase with dose of ACh, whereas nerve-evoked responses have time-courses independent of the number of vagal stimuli.

The peak response of the muscle increases as the iontophoretic dose of ACh (in nanocoulombs) is increased. The relationship between dose and peak response (Fig. 5 *a*) is linear over only a very small range (up to ~2 mV peak hyperpolarization).

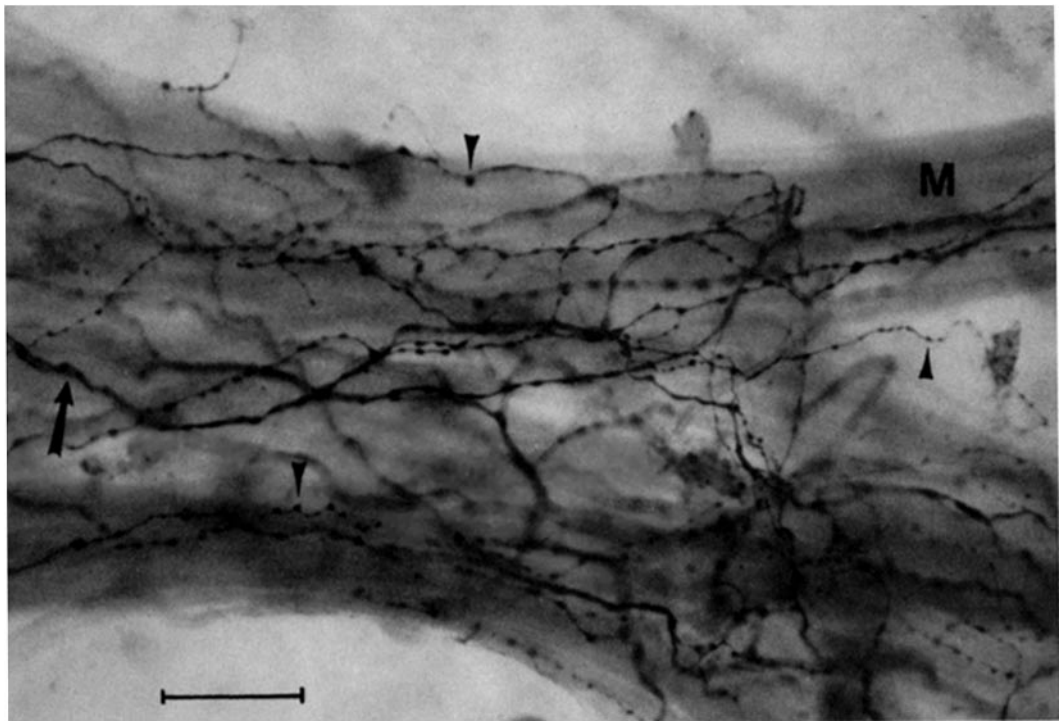

FIGURE 2 Portion of frog interatrial septum stained with zinc iodide and osmium. Numerous varicosities (arrowheads) and bundles of axons (arrow) are seen on the surface of muscle fibers (*M*) and in the extracellular spaces. Bar, 20 μm.

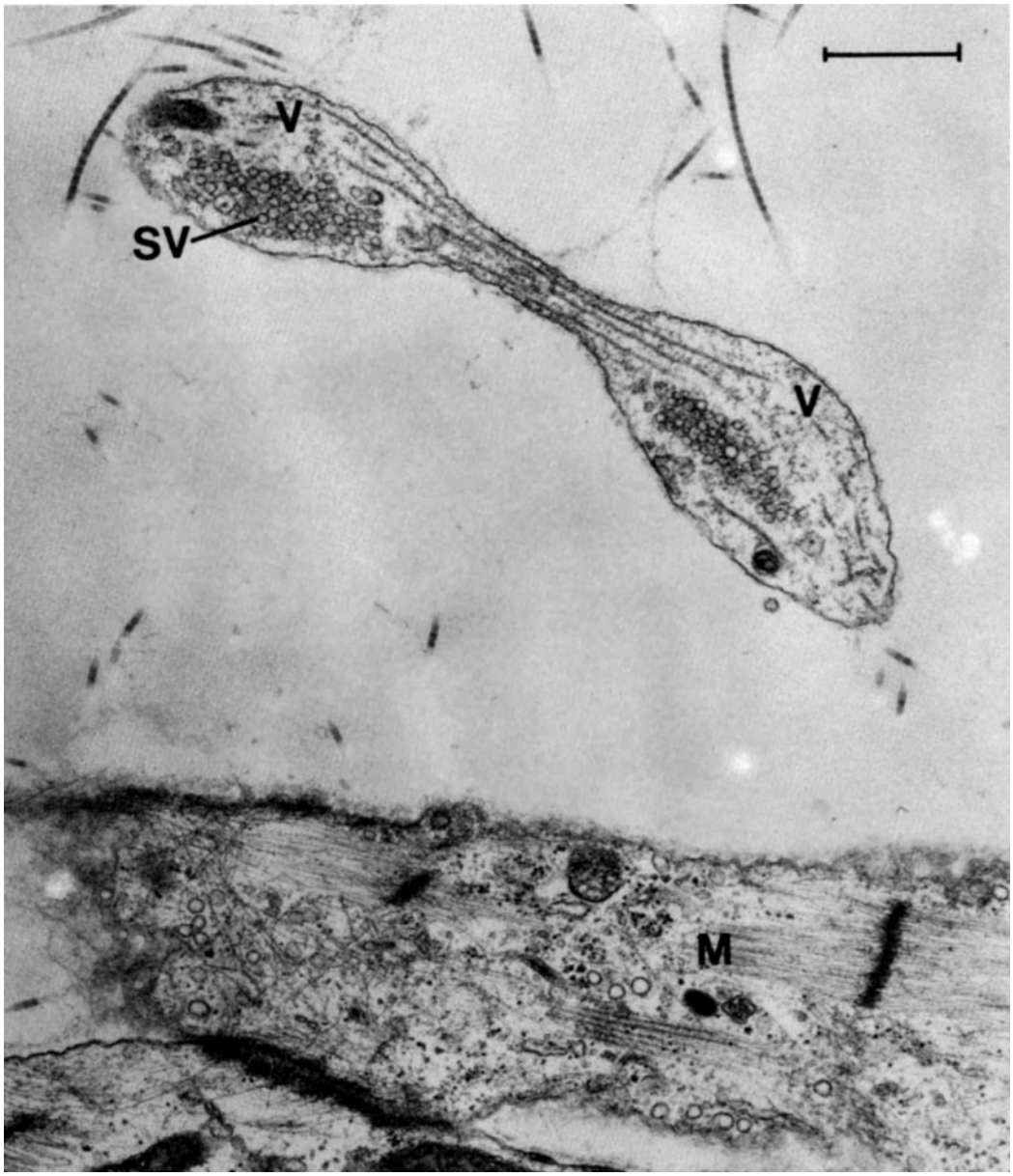

FIGURE 3 Electron micrograph of autonomic varicosities in the interatrial septum. Two varicosities (*V*) containing many clear synaptic vesicles (*SV*) are seen located several micrometers from the nearest cardiac muscle fiber (*M*). Bar, 1 μm.

From the initial linear portion of Fig. 5 *a*, the chemosensitivity was estimated to be 13.5 mV/nC. Above 2 mV, the dose-peak response relationship saturates, possibly as a result of local saturation of receptors at the tip of the ACh pipet. With increasing doses of ACh, both the times to peak and half-decay times of the responses become progressively longer (Fig. 4 *a*). This suggested that the time integral of the response might be more directly related to ACh dose. In Fig. 5 *b*, the time integral of the responses in Fig. 5 *a* are shown to be linearly related to ACh dose over the entire range examined. The ACh sensitivity of this fiber, expressed as the time integral response is 33 mV · s per nanocoulomb. The prolonged time-course of responses to large ACh doses might be the result of local saturation of receptors at the tip of the ACh pipet and lateral diffusion of ACh into adjacent areas.

Responses to iontophoretic ACh invariably begin with a latency of >50 ms. This latency was not a result of diffusion of ACh to distant receptors: the ACh pipet was positioned visually onto the impaled muscle fiber within several micrometers of the recording electrode. Lateral adjustments of the pipet position along the fiber had no influence on latency or time-course of the response. Furthermore, the time-course and the latency of the response were markedly temperature dependent. As shown in Fig. 6, reduction of the temperature from 28° to 18°C increased the latency of the response from 100 to 275 ms and increased the time to peak from 1 to 1.4 sec. This temperature dependence provides further evidence that the latency was not a result of simple diffusion of ACh to distant receptors. Similar results have been reported by Pott (48) (see Discussion).

Mapping ACh Sensitivity

ACh sensitivity of various spots along the muscle fiber was determined by constructing a dose-response curve (as in Fig. 5) at several spots on a muscle fiber. Small doses of ACh were used such that the peak response vs. dose relationship was in the linear range. In the fiber shown in Fig. 7, the sensitivities

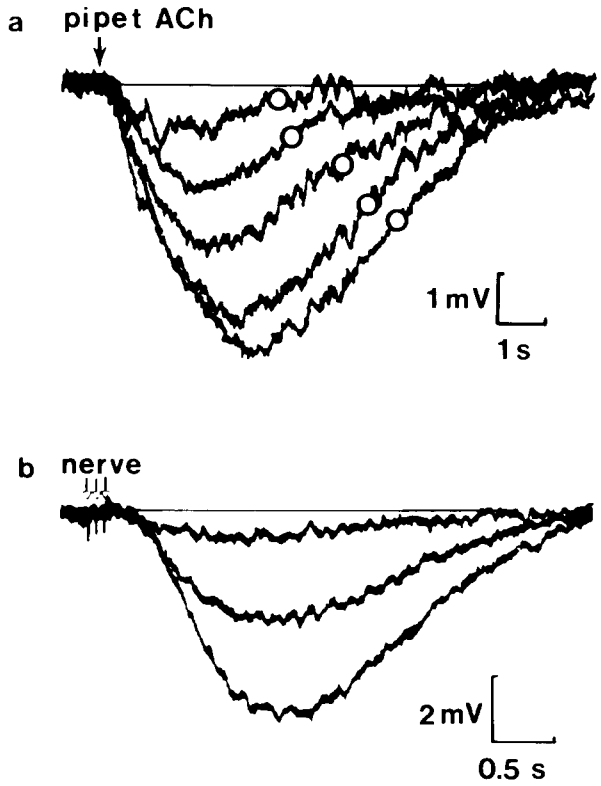

FIGURE 4 Responses of sinus venosus muscle fiber to nerve-released and iontophoretic ACh. *(a)* Five superimposed responses produced by 22-, 42-, 65-, 135-, and 170-nA 5-ms duration pulses of ACh from an iontophoretic pipet. Preparation bathed in 4 mM Mn Ringer's. Open circles (O) indicate half-decay times. *(b)* Three superimposed responses produced by stimulating vagus nerve with 1, 2, or 3 impulses. Preparation bathed in normal Ringer's containing 1 μg/ml D600 to suppress spontaneous beating and 1 μM propranolol to block sympathetic effects.

of six spots on or near the fiber were measured. The sensitivities of spots *C–F* on the fiber were very similar (range: 28–32 mV/nC). Thus, within the resolution of the technique, ACh receptors are not clustered in cardiac muscle membrane. The large doses of ACh that were required to produce measurable responses and the slow time-course of the responses, however, suggested that the spatial resolution of this technique might not be adequate to resolve differences in sensitivity on a micron scale. Several tests were made to estimate the spatial resolution of the iontophoretic mapping technique.

The iontophoretic pipet was positioned 10–25 μm away from the edge of the muscle fiber, and responses to pulses of ACh were examined. The muscle fiber in Fig. 7 responded to pulses of ACh even when the ACh pipet was placed 25 μm away from the edge of the fiber (Fig. 7*A*). However, the peak response was significantly attenuated and the latency of the response was increased markedly (from 110 to 230 ms). When the iontophoretic pipet was 10 μm from the edge of the fiber (Fig. 7*B*), the response was very similar in amplitude and time-course to that seen when the pipet touched the fiber, but the latency was slightly prolonged (from 110 to 140 ms). When the iontophoretic pipet was raised 5–10 μm above the endothelial layer covering the muscle, no responses were seen, even to large iontophoretic pulses.

These results suggest that the iontophoretic technique has a resolution of 10–25 μm at best. If ACh receptors were clustered in patches separated by <25 μm, this technique might not reliably detect spatial differences in sensitivity. For this reason, another method was devised to examine receptor distribution.

Characterization of QNB Binding Sites in Heart Homogenates

The distribution of mAChR in heart was examined by studying the binding of the muscarinic antagonist, [^{3}H]QNB. To use this ligand as a tag for the ACh receptor, it was first necessary to demonstrate that QNB binds saturably to one class of binding sites with a high affinity and that this binding exhibits the pharmacological characteristics of the ACh receptor.

The first series of experiments characterized the equilibrium dissociation constant (K_d) and the on and off rates of [^{3}H]QNB binding to homogenates of whole *Xenopus* heart. Determinations were made at 21°C, the body (ambient) temperature of these animals, and at 37°C for comparison to data on mammalian mAChR in the literature.

The equilibrium binding of (−) [^{3}H]QNB to heart homogenates was measured as a function of free (−) [^{3}H]QNB concentration. An example of data obtained at 21°C is shown in Fig. 8. Similar data were obtained at 37°C. Total [^{3}H]QNB binding exhibited a specific and a nonspecific component. The specific component was defined as the difference in the binding of

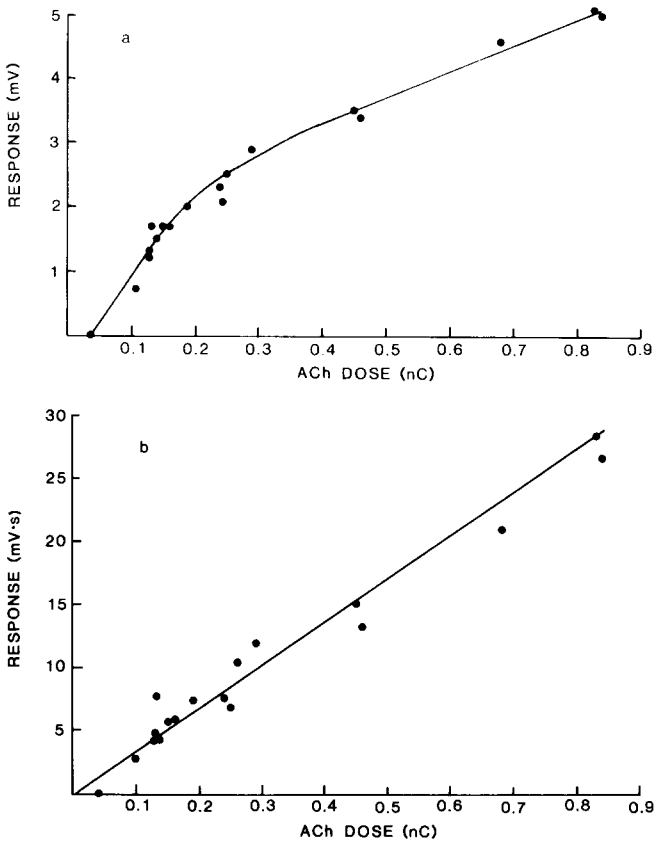

FIGURE 5 Dose-response relationship of a muscle fiber in the sinus venosus. *(a)* 5-ms-duration pulses of ACh were delivered from an iontophoretic micropipet placed on a muscle fiber within 50 μm of the recording electrode. The amplitude of the iontophoretic pulse was varied and duration maintained constant. The peak hyperpolarization is plotted as a function of dose of ACh in nC. Sample traces from this series are shown in Fig. 4. *(b)* The areas of the responses in *a* were measured and the areas (in millivolts times seconds) are plotted as a function of ACh dose.

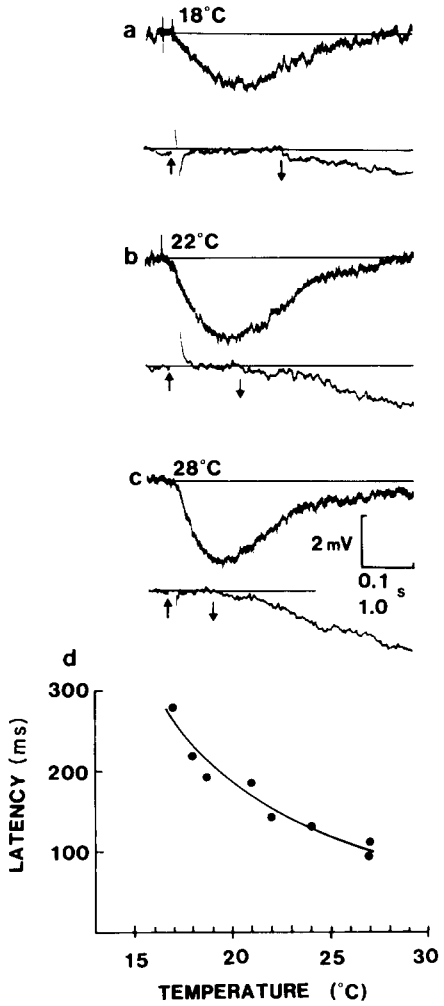

FIGURE 6 Temperature sensitivity of ACh hyperpolarization. The responses produced by iontophoretic pulses of ACh 10 ms in duration were examined during perfusion of the preparation chamber with chilled or warmed Ringer's. Temperature was measured by a miniature temperature probe mounted in the center of the chamber. Representative traces shown were recorded at (*a*) 18°, (*b*) 22°, and (*c*) 28°C. Upper traces in each panel show responses on a slow time-base (1 s/bar); lower traces are the same response on a fast time-base (0.1 s/bar). Latencies were measured from the start of the voltage artifact of the iontophoretic pulse (upward arrow) to the first point at which the trace departed from the baseline (downward arrow). *(d)* Plot of the experiment illustrated in part in *a–c* Each point represents the average latencies of two to three responses.

[^{3}H]QNB in the presence and absence of 1 μM atropine or 10 nM unlabeled (±) QNB. The specific binding isotherm resembled a rectangular hyperbola. Specific binding sites were saturable at low concentrations (~0.1 nM) of (−) [^{3}H]QNB. When linearized according to the method of Scatchard (52) (Fig. 8*b*), these data are well fitted by a single straight line (correlation coefficients of 10 experiments averaged 0.96). These results show that QNB binds specifically to a single, saturable class of receptors. The K_d for QNB binding, determined by Scatchard analysis, was 11.1 ± 1.6 pM at 37°C and 11.5 ± 1.6 pM at 21°C (mean ± standard deviation, $n = 5$ at 21°C and $n = 4$ at 37°C). Lower-affinity, specific binding sites for QNB were not observed, even when free (−) [^{3}H]QNB concentration was increased to 1 nM. Nonspecific binding in the presence of 1 μM atropine or 50 nM unlabeled (±) QNB was not saturable and comprised <10% of the total binding at concentrations of (−) [^{3}H]QNB (0.2 nM) that saturated specific binding sites.

The association rate of QNB binding was determined by measuring the binding of [^{3}H]QNB as a function of time at several different [^{3}H]QNB concentrations (data for 21°C shown in Fig. 9). The rate of QNB binding increases with increasing [^{3}H]QNB concentration. At 0.56 nM (±) [^{3}H]QNB, 90% of the receptors are bound in 60 min. If the binding of QNB is a simple bimolecular reaction with a single class of receptors, a semilogarithmic plot of the fraction of unbound receptors ($LR_e - LR_t/LR_e$) vs. time should be a straight line. When the data of Fig. 9*a* are replotted in this way (Fig. 9*b*), however, it is seen that the binding occurs with two different rates. Analogous results were obtained at 37°C except that the rate of binding was faster. The kinetics of QNB binding are not consistent with a simple bimolecular reaction. Galper et al. (12), who have reported a similar phenomenon with muscarinic receptors from embryonic chick heart, suggest that the nonlinearity in semilogarithmic plots of $LR_e - LR_t/LR_e$ vs. time represents a two-step reaction of QNB binding to a single class of receptors rather than QNB binding to two different sites. My results also are consistent with two-step binding. The fraction of sites that bind QNB slowly can be estimated by extrapolating the slowly associating components of the lines in Fig. 9*b* to time 0. The fraction of slowly associating sites increases from 10% to >60% as (±) [^{3}H]QNB concentration is increased from 0.04 to 0.56 nM. This observation is inconsistent with two independent binding sites. Further support for a two-step binding process is obtained from dissociation experiments (below).

The dissociation rate constant was determined by measuring the decrease in bound [^{3}H]QNB after adding unlabeled competitor (50 nM unlabeled (±) QNB or 100 μM oxotremorine). In experiments in which homogenates were incubated 90 min in [^{3}H]QNB before addition of competitor, [^{3}H]QNB appeared to dissociate at a single exponential rate that was temperature dependent (Fig. 10*a*). Although some variability was noted in dissociation rates between experiments, the following dissociation rate constants from a single experiment were typical: 7×10^{-3}/min at 37°C, 3×10^{-3}/min at 30°C and 1.2×10^{-3}/min at 21°C. At 4°C, dissociation was very slow, with a rate constant $< 6 \times 10^{-4}$/min. If the homogenate was incubated at 21°C for only 5 min before addition of competitor, dissociation often occurred with two rates (Fig. 10*b*). The quickly dissociating component was so small or dissociated so quickly at 37°C that it was not usually seen. At 21°C, ~60% of the bound [^{3}H]QNB dissociated with a $t_{1/2}$ of ~7 min. These observations are consistent with a two-step mechanism for QNB binding to its receptor. [^{3}H]QNB first forms a quickly associating and dissociating complex that is slowly converted into a slowly dissociating complex. Thus, after short exposures to [^{3}H]QNB both the quickly and slowly dissociating complexes are seen, whereas after long exposures all of the QNB-receptor complexes have been converted to the slowly dissociating form. Because most experiments in this paper examine [^{3}H]QNB binding at equilibrium after long exposures to [^{3}H]QNB, [^{3}H]QNB may be considered simply to be binding to a single high-affinity site.

The pharmacological specificity of QNB binding was investigated by examining the ability of various cholinergic drugs to complete for [^{3}H]QNB binding. Various concentrations of competitor were added to solutions of 0.5 nM (±) [^{3}H]QNB, and the binding assay was initiated by addition of heart homogenate. After a 90-min incubation at 21°C, the bound [^{3}H]QNB

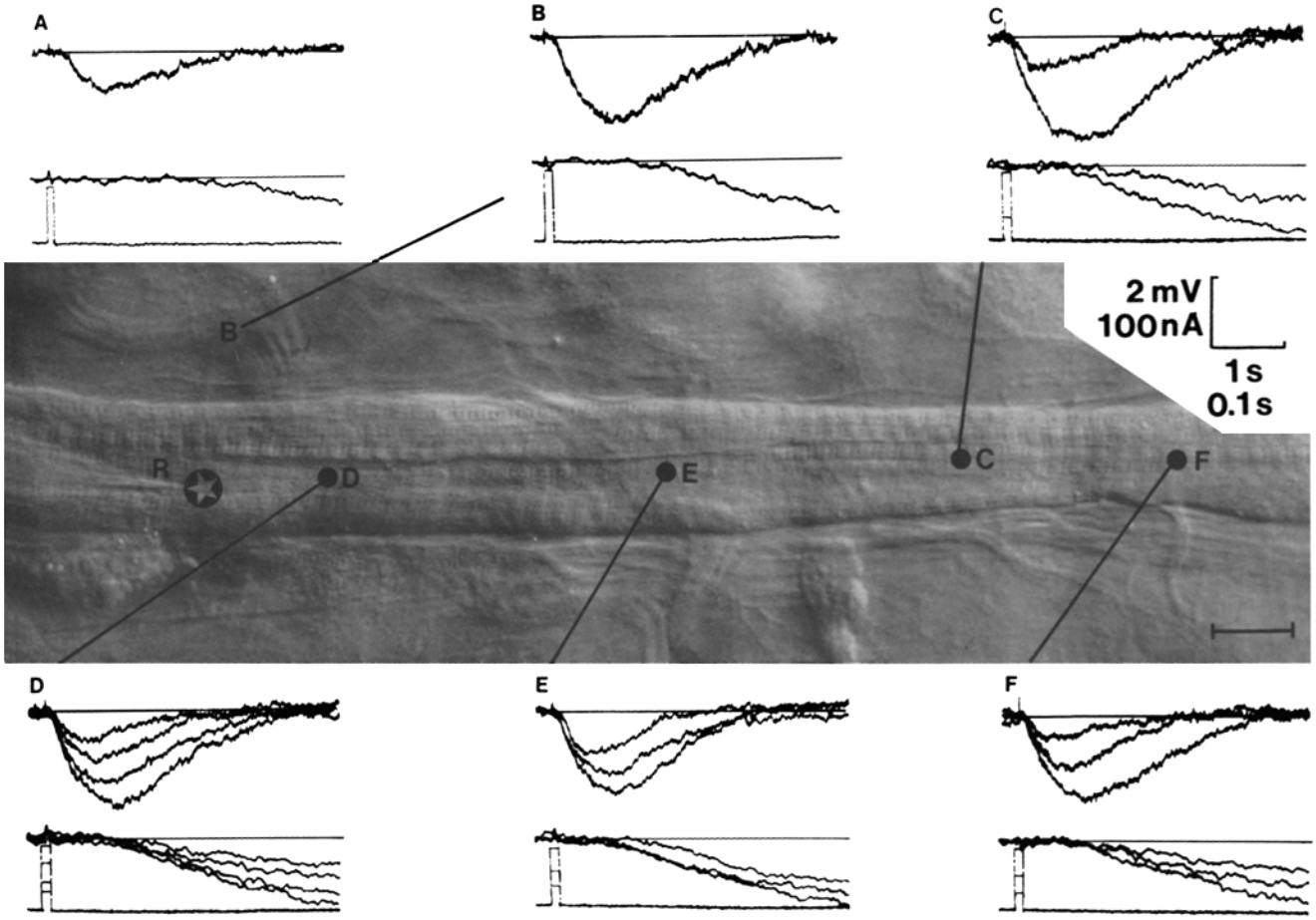

FIGURE 7 Iontophoretic mapping of ACh sensitivity of a muscle fiber in the sinus venosus. The ACh pipet was positioned at six different spots (*A–F*) on or near the muscle fiber shown in the micrograph. The preparation was viewed with Nomarski differential interference contrast optics to permit accurate positioning of the pipet. The recording electrode (*R*) can be seen entering the left of the field and penetrating the fiber at the star. The muscle fiber is somewhat vacuolated as a result of the prolonged penetration preceding this photograph. In each panel of oscilloscope traces (*A–F*), top traces show the response of the muscle to pulses of ACh. Often several responses are superimposed. Middle traces show the same responses on a faster time-base to illustrate the latency. Bottom traces show the iontophoretic pulses. Bottom traces are retouched. The iontophoretic pipet was positioned (*A*) 25 μm from the edge of the fiber (position not shown on micrograph), (*B*) 10 μm from edge of fiber, (*C–F*) touching the muscle fiber as shown in the micrograph. Bar, 10 μm.

was determined by filtration and plotted as a function of competitor concentration. Competition curves for the muscarinic antagonists QNB, atropine, and tropicamide and the agonists oxotremorine, ACh, carbamylcholine (CCh), and bethanechol (BCh) are shown in Fig. 11. The following IC_{50} values (the concentration of competitor that blocked 50% of the [^{3}H]QNB binding) were found: QNB, 5×10^{-10} M; atropine, 3×10^{-9} M; tropicamide, 3×10^{-7} M; oxotremorine, 1.5×10^{-6} M; ACh, 10^{-5} M; CCh, 10^{-4} M; BCh, 4×10^{-4} M. Analysis of the competition data by the method of Brown and Hill (6) confirmed previous studies that antagonists have higher Hill coefficients than agonists have. The following Hill coefficients were obtained: QNB, 1.05; atropine, 0.89; tropicamide, 0.83; oxotremorine, 0.67; ACh, 0.49; CCh, 0.51; BCh, 0.53.

The ability of various muscarinic drugs to compete for QNB binding provides strong support for the contention that QNB binds to muscarinic ACh receptors. Further support was provided by the finding that the order of potency of agonists to compete for QNB binding (oxotremorine > ACh > CCh > BCh) reflected the ability of the agonists to hyperpolarize muscle cells in the sinus venosus. Fig. 12 illustrates responses of a muscle fiber to bath-applied agonists. In the absence of inhibitors of acetylcholinesterase, oxotremorine is more potent than ACh or CCh. ACh and CCh have similar potencies and BCh is quite ineffective in producing a hyperpolarization. With neostigmine, an inhibitor of acetylcholinesterase (Fig. 12*e*), however, the response to ACh is markedly potentiated such that ACh is only slightly less potent than oxotremorine.

Distribution of QNB Binding Sites in Heart

The concentration of QNB binding sites in different chambers of the frog heart was determined by Scatchard analysis of equilibrium [^{3}H]QNB binding to homogenates. In Fig. 13, bound [^{3}H]QNB is in units of femtomoles per milligram of protein such that the *x*-axis intercept represents concentration of receptor in the tissue. Receptor concentrations were found to be higher in atria and sinus than in ventricle (Table I). The K_d of QNB binding to receptors from the various chambers of the frog heart were similar (Table I).

QNB Binding Sites in Intact Cells

The experiments with homogenates demonstrated the presence of a high-affinity, saturable QNB binding site in heart.

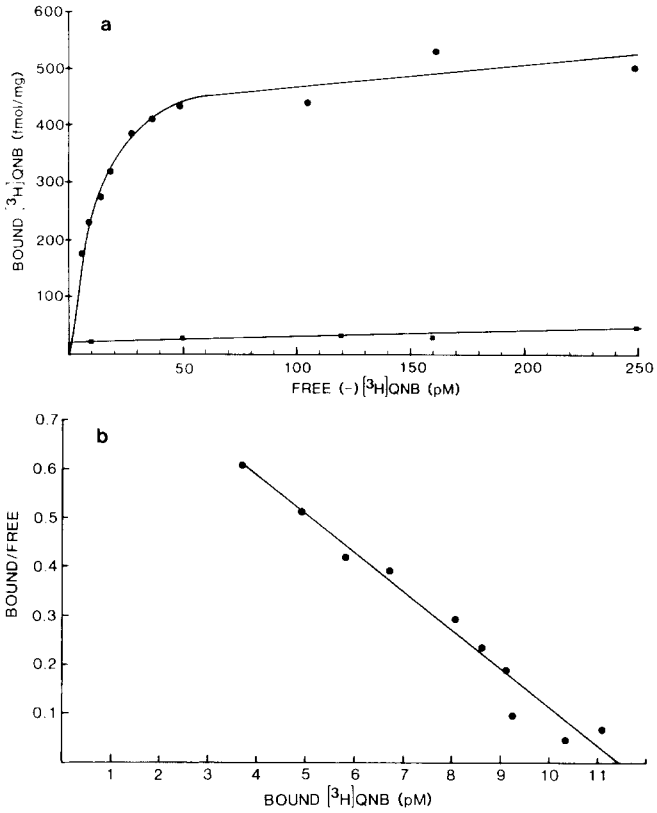

FIGURE 8 Equilibrium binding of [^{3}H]QNB to homogenates of whole frog heart. *(a)* Aliquots of homogenates of frog heart were incubated in various concentrations of (±) [^{3}H]QNB for 4 h at 21°C. Bound (−) [^{3}H]QNB was determined as described in Materials and Methods. Free (−) [^{3}H]QNB concentration was calculated assuming that 50% of the (±) [^{3}H]QNB was active (−) isomer and subtracting bound (−) [^{3}H]QNB from total (−) [^{3}H]QNB. Nonspecific binding (■) was determined by parallel incubations in the presence of 50 nM unlabeled (±) QNB. Specific binding (●) was determined by subtracting nonspecific from total binding. In this experiment, the 2 ml assay mixtures contained 41.8 μg Lowry protein. Receptor concentration was 11.4 pM. *(b)* Scatchard plot of specific binding in *a*. Ordinate is bound/free [^{3}H]QNB concentrations, abscissa is bound [^{3}H]QNB in pmol/liter. Correlation coefficient was 0.98. The K_d at 21°C was 12.6 pM as determined by the slope of the Scatchard plot. Lines are drawn by use of nonweighted least squares.

The next series of experiments was designed to compare the characteristics of QNB binding sites in intact tissue to those in homogenates. Small pieces of living *Xenopus* atrium (~2 mg of protein) were incubated with (±) [^{3}H]QNB to equilibrium (4–12 h) at 21°C and washed, and the amount of bound (−) [^{3}H]QNB was plotted as a function of free (−) [^{3}H]QNB concentration. The binding isotherm (Fig. 14) resembles a rectangular hyperbola. The data are fitted by straight line on Scatchard analysis with a correlation coefficient of 0.87 (*inset*, Fig. 14). This relatively poor fit is probably the result of large variability in binding of QNB to intact tissue pieces. The binding isotherm from intact tissue (Fig. 14) differs somewhat from that obtained with tissue homogenates. The K_d determined from the Scatchard plot is 148 pM. This K_d is an order of magnitude larger than that found for homogenates (11.5 pM at 21°C). This large K_d is not attributed to failure to reach equilibrium, because incubation of the tissue in [^{3}H]QNB for 4 or 12 h gave similar levels of specific QNB binding. The difference in K_d between homogenates and intact tissue is not understood and requires further study. The concentration of receptors in intact binding experiments is 891 fmol/mg. This is virtually the same as the receptor concentration measured in atrial homogenates (Table I). Nonspecific binding to intact cells in the presence of 100 μM atropine was similar to that in tissue homogenates. In the experiment illustrated in Fig. 14, ~5% of the total binding was nonspecific at (−) [^{3}H]QNB concentration of 1.0 nM.

As with tissue homogenates, [^{3}H]QNB dissociated slowly from receptors in intact tissue. At 4°C, virtually no dissociation of [^{3}H]QNB was detected over a period of 24 h (Fig. 15). Glutaraldehyde fixation had no effect on dissociation rate of [^{3}H]QNB from intact tissue pieces (Fig. 15).

Effect of QNB on the ACh Response

To determine further the concentration of QNB required to saturate ACh receptors in the intact tissue, the effect of various QNB concentrations on the hyperpolarization produced by ACh in sinus venosus was examined. The responses to iontophoretically applied ACh or nerve stimulation were recorded from muscle fibers before and during exposure to (±) QNB applied to the bath. In all cases, 1–5 nM (±) QNB reduced the peak hyperpolarization >90% in <1 h. 0.5 nM (±) QNB reduced the responses to 65–80% of the control value in 1–2 h. At this time it appeared that a steady state had been attained. 2 h Exposure to 0.05 nM QNB had little or no effect on the amplitude of the response.

Distribution of QNB Binding Sites on Single Fibers

The distribution of QNB binding sites on muscle fibers was determined by autoradiography of whole mounts of frog interatrial septum and sinus venosus. These tissues are ideally suited for autoradiography because they are very thin sheets. Fig. 16 illustrates several fields of an autoradiograph of a muscle fiber

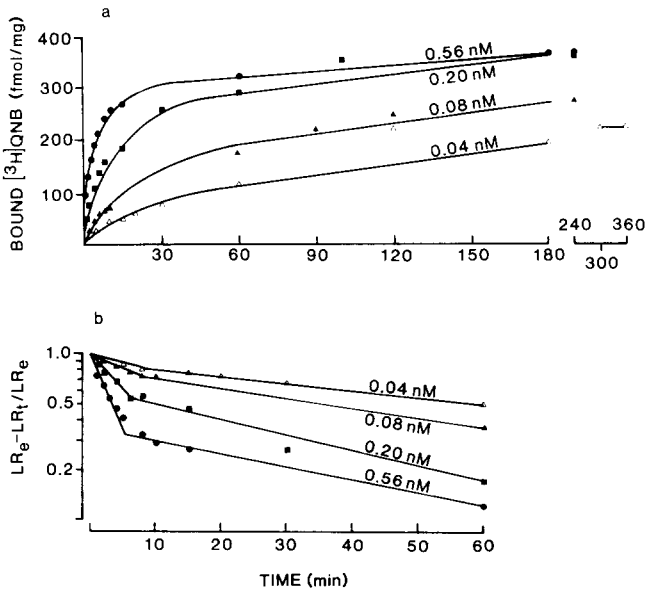

FIGURE 9. The rate of formation of QNB-receptor complexes. Aliquots of whole heart homogenate were incubated in 0.04 (△), 0.08 (▲), 0.20 (■), or 0.56 nM (●) (±) [^{3}H]QNB for the times indicated on the abscisa. Bound [^{3}H]QNB was measured as described in Materials and Methods. (*a*) Linear coordinates, (*b*) data in *a* replotted according to Eq. 5 in Materials and Methods. Lines are drawn by eye.

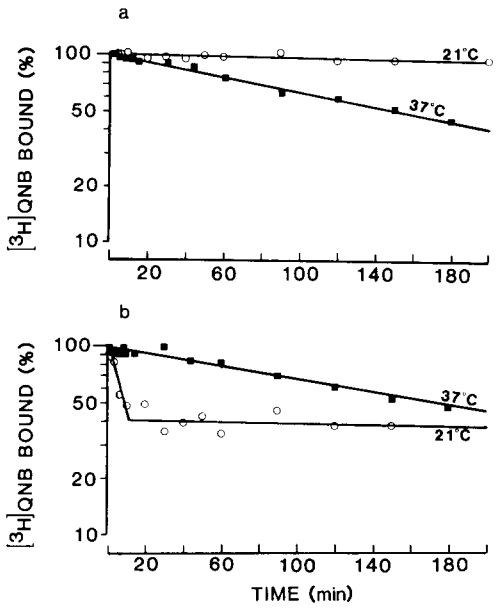

FIGURE 10 Dissociation of [^{3}H]QNB. Heart homogenate was incubated in the presence of 0.5 nM (±) [^{3}H]QNB for 90 min (*a*) or 5 min (*b*) at 37°C (■) or 21°C (○). At the end of the incubation, competitor was added to the tube and the incubation continued for the time indicated on the abscissa. Bound [^{3}H]QNB was then determined as described in Materials and Methods. Competitor was 100 μM oxotremorine for the 21°C experiment and 50 nM unlabeled (±) QNB for the 37°C experiment. Similar results were obtained with other competitors.

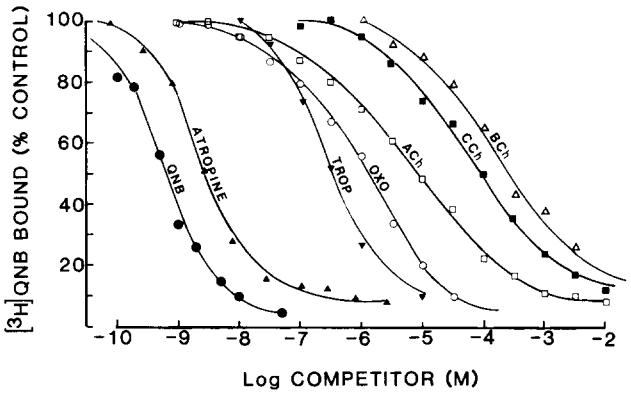

FIGURE 11 Competition of various cholinergic agonists and antagonists for [^{3}H]QNB binding. Aliquots of heart homogenates were incubated with 0.5 nM (±) [^{3}H]QNB for 90 min in the presence of the indicated concentrations of unlabeled QNB (●), atropine (▲), tropicamide (▼), oxotremorine (○), acetylcholine (□), carbamylcholine (■), or β-methylcarbamylcholine (bethanechol), (△). Bound [^{3}H]QNB was measured as described in Materials and Methods and expressed as a percent of that bound in the absence of competitor. 3×10^{-6} M neostigmine bromide was present in the acetylcholine competition assay.

in the interatrial septum labeled with [^{3}H]QNB. Silver grains are distributed over the entire surface of the muscle fiber. In this preparation, the density of silver grains over the fibers was 0.07 grains/μm^2. Because the silver grains are highly localized to muscle fibers, little diffusion of the label has occurred during processing. Nonspecific binding was measured in preparations that were incubated in [^{3}H]QNB in the presence of 100 nM unlabeled QNB (Fig. 16*d*). Nonspecific grain densities over muscle fibers were not significantly different from background (0.01 grains/μm^2). The distribution of silver grains over all fibers in a given preparation is similar (Fig. 16*a*). The distribution of silver grains over fibers in the sinus venosus is similar to that seen in the interatrial septum. Preparations labeled with 0.2 nM (±) [^{3}H]QNB had a lower level of binding but the grain distributions were similar to those seen when tissue was labeled with 2.5 nM (±) [^{3}H]QNB.

Examination of autoradiographic preparations never revealed "hot spots" of grain density or any regular clumping of silver grains. Indeed, it appeared that the grain distribution was random in nature. Because the silver grains are produced by a random radioactive decay, a uniform distribution of QNB binding sites would be revealed as a random distribution of silver grains in the autoradiogram. In my preliminary report (21), evidence was presented that grain distributions are random.

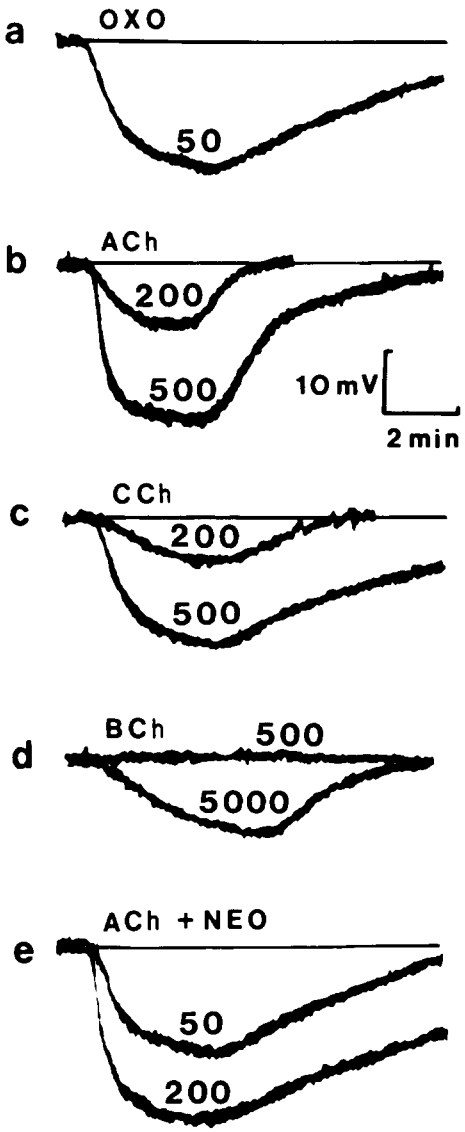

FIGURE 12 Responses of sinus venosus muscle fiber to muscarinic agonists. Agonists were applied by addition to the medium bathing the preparation; (*a*) 50 nM oxotremorine, (*b*) two superimposed responses to 200 nM and 500 nM acetylcholine, (*c*) two superimposed responses to 200 nM and 500 nM carbamylcholine, (*d*) two superimposed responses to 500 nM and 5000 nM bethanechol, (*e*) two superimposed responses to 50 nM and 200 nM acetylcholine taken 30 min after addition of 3×10^{-6} M neostigmine bromide.

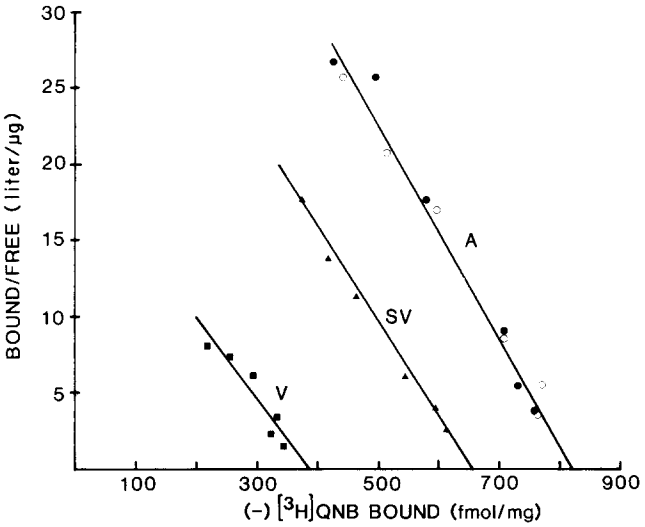

FIGURE 13 Scatchard analysis of [^{3}H]QNB binding to different chambers of frog heart. Frog hearts were dissected into sinus venosus (▲), left atrium (○), right atrium (●), and ventricle (□), and homogenized. The equilibrium [^{3}H]QNB binding to aliquots of these homogenates was measured as in Fig. 8. The units of this Scatchard plot differ from those of Fig. 8 *b*. In this figure, bound [^{3}H]QNB is expressed in femtomoles per milligram of protein (in Fig. 8 *b*, bound [^{3}H]QNB is in picomoles per liter). The *x*-intercept gives the concentration of receptors (in femtomoles per milligram) in the tissue. Receptor concentrations in the assay were: sinus, 19.5 pM; left atrium, 29.3 pM; right atrium, 31.7 pM; ventricle, 10.7 pM. Sinus and atrial pieces from nine frogs were pooled for each Scatchard analysis. Lines calculated by nonweighted least squares analysis. The line drawn through the atrial points (○, ●) is for data only from right atrium (●).

TABLE I

QNB Binding Sites in Heart Chambers

Chamber	Receptor concentration*	K_d‡
	(fmol/ mg protein)	*(pM)*
Sinus venosus	654	16.6
Right atrium	819	13.8
Left atrium	841	15.3
Ventricle	384	19.1

* Receptor concentration determined by extrapolation of Scatchard plots in Fig. 15 to *x*-axis. Concentration of receptors in sinus venosus muscle is expected to be higher than value given, because the fraction of connective tissue in sinus is very high compared to other chambers.

‡ K_d was determined from nonweighted least-squares slope of Scatchard plots of Fig. 13. Correlation coefficients were 0.99 for all but ventricle, which was 0.94.

DISCUSSION

The main finding of this study is that cardiac muscle fibers are uniformly sensitive to ACh over their entire surface. This uniform distribution correlates well with the distribution of QNB binding sites that correspond to mAChR.

Organization of Neuroeffector Junctions in Heart

It is well recognized that the neuroeffector junctions in many autonomically innervated tissues are relatively unspecialized. In the heart, the postganglionic nerve fibers form a widely ramifying network or plexus over the muscle (1, 17, 26, 28, 29, 57, 58). The terminal axons are composed of chains of varicosities. Although direct evidence is lacking, these varicosities are thought to be *en passage* sites of transmitter release, mainly because they contain dense accumulations of synaptic vesicles (17). Varicose axons sometimes pass near the muscle, but in many cases the varicosities are separated from the nearest target by a space of several micrometers or more (for example, Fig. 1). Searches for nerve-cardiac muscle junctions with the electron microscope have usually revealed few close associations of the presynaptic and postsynaptic membranes (for examples, see references 17, 18, and 45), although some close appositions have been reported (36, 54–56). Even in cases where close appositions of pre- and postsynaptic membranes have been seen, the postsynaptic membrane seldom exhibits obvious structural differences form the nearby sarcolemma.

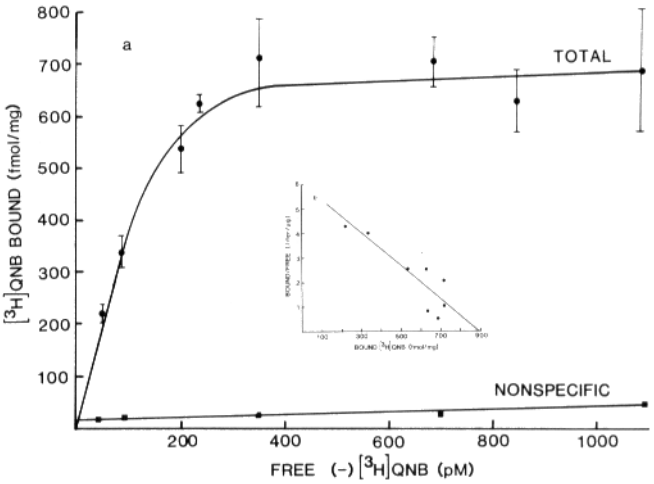

FIGURE 14 (*a*) Equilibrium [^{3}H]QNB binding to intact pieces of atrium. Small pieces of atrium (~2 mg protein) were incubated in various concentrations of [^{3}H]QNB at 21°C in Ringer's for 12 h, washed with numerous changes of Ringer's for 2 h, and homogenized in 0.1 N NaOH. Aliquots were removed for determination of bound [^{3}H]QNB and Lowry protein. Nonspecific binding was determined on pieces incubated in [^{3}H]QNB and 100 μM atropine. Each point is the mean (± SD) of four to eight atrial pieces. *Inset* (*b*), Scatchard plot.

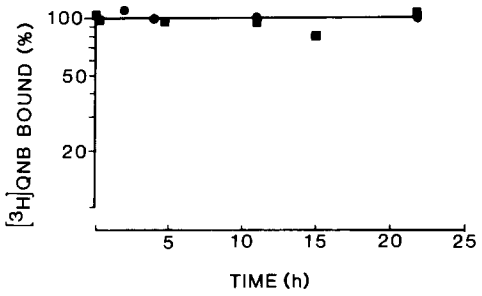

FIGURE 15 Dissociation of [^{3}H]QNB from intact pieces of atrium. (●) Dissociation from fresh tissue. Small pieces of atrium were incubated in 2.5 nM (±) [^{3}H]QNB for 4 h at 21°C, rinsed many times in Ringer's for 2 h at 4°C, and then incubated in 100 nM unlabeled (±) QNB at 4°C (time = 0). At various times, pieces were removed for determining bound [^{3}H]QNB. (■) Dissociation from glutaraldehyde-fixed tissue. Pieces were incubated in [^{3}H]QNB at 21°C as above, and rinsed at 4°C. Four samples were removed for determining bound [^{3}H]QNB after 30 min of washing (time = 0). The remaining samples were fixed in 1% glutaraldehyde buffered with sodium phosphate, pH 7, for 30 min and rinsed. Samples of glutaraldehyde-fixed tissue were taken at various intervals for determining bound [^{3}H]QNB. Each point is the mean of four to five atrial pieces.

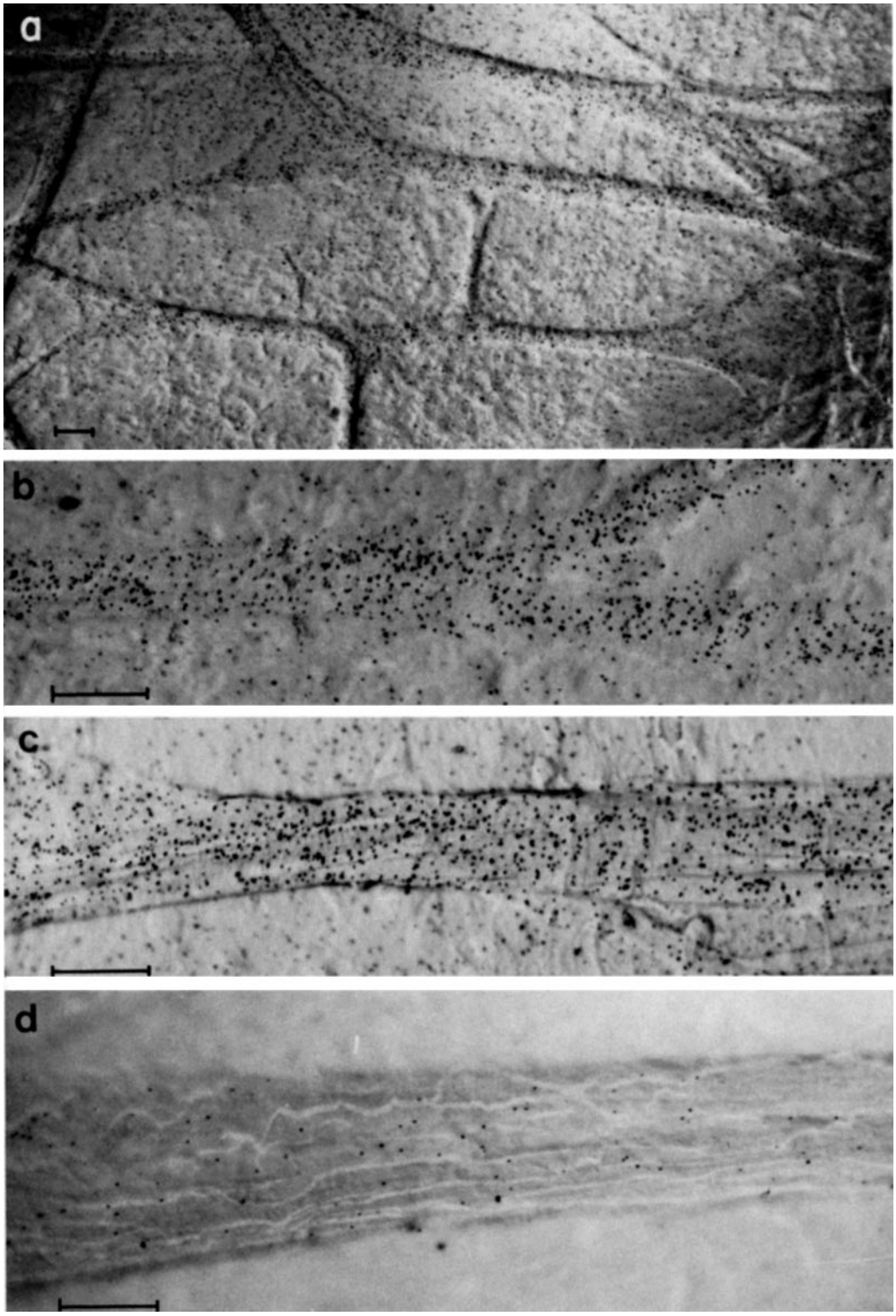

FIGURE 16 Autoradiograph of portion of interatrial septum labeled with [^{3}H]QNB. Interatrial septa were incubated in 1.5 nM (±) [^{3}H]QNB (29.4 Ci/mmol) in frog Ringer's solution for 2.5 h at 21°C, washed with numerous changes of ice-cold Ringer's for 2 h, fixed for 30 min in 1% glutaraldehyde buffered with sodium phosphate, pH 7, and washed in Ringer's for an additional 10 h. Thin portions of the septa were cut out and prepared for autoradiography as described in Materials and Methods. (*a*) Low-power view to illustrate labeling pattern. (*b* and *c*) High-power views to show grain distribution on single fibers. (*d*) Nonspecific binding in the presence of 100 nM unlabeled (±) QNB. Bars, 50 μm.

The present study demonstrates further that the postsynaptic membrane of the cardiac muscle fiber is not highly specialized on a molecular level. ACh sensitivity was found by iontophoretic mapping to be distributed uniformly on fibers in the sinus venosus. Difficulties were encountered, however, in achieving a resolution of <10–25 μm with this technique. Poor resolution was largely the result of the large pulses of ACh required to produce measurable responses, the absence of highly localized

acetylcholinesterase in the postsynaptic membrane to limit the lateral diffusion of the ACh, and the slow time-course of the response.

Binding of QNB to receptors was used to characterize further the distribution of mAChR. Evidence was presented that QNB binds to mAChR. (*a*) QNB binds with high specificity to a single, high-affinity, saturable site. (*b*) QNB blocks the response of the heart to muscarinic agonists. (*c*) [^{3}H]QNB binding is competed by muscarinic agonists and antagonists. The ability of agonists to compete for binding is paralleled by the potency of the agonists to produce a response in the cardiac muscle. These data confirm and extend observations of other laboratories on QNB binding sites in other heart systems (7, 11, 12, 59).

The distribution of QNB binding sites, like that of the ACh sensitivity, was found to be random, at least over short lengths of muscle fiber. Gradations in the density of QNB binding sites were seen in different regions of the interatrial septum, but no regular differences were seen from animal to animal. Regular differences exist, however, in the density of mAChR in various chambers of the heart (Fig. 13). These differences correspond fairly well to differences in the density of innervation as determined by ZIO staining: the sinus and atria have both higher levels of QNB binding sites and more autonomic varicosities than the ventricle. In mammalian hearts, the sinoatrial (SA) node and atria are more sensitive to ACh than the ventricles (25, 29, 38).

The conclusion that ACh receptors are uniformly distributed on the surface of cardiac muscle cells depends on two assumptions. The first assumption is that QNB binding sites visualized by autoradiography are located on the cell surface. This assumption seems justified for several reasons. (*a*) Nonspecific binding, which would include uptake into the cell, is <10% (Fig. 14). (*b*) The energy of the β emission from ^{3}H is low, and intracellular sites >1 μm from the surface are unlikely to be registered by the emulsion. I cannot exclude the possibility, however, that [^{3}H]QNB binds specifically to intracellular sites, some of which are registered by the emulsion. Because the number of sites labeled in intact cells is similar to that in homogenates (c.f., Figs. 13 and 14), the presence of a large intracellular pool of receptors seems to be excluded. The second assumption in the autoradiographic experiments is that no diffusion of QNB occurs during processing of the tissue. Diffusion of QNB seems unlikely because the silver grains are highly localized to the muscle fibers (Fig. 16). It is unlikely that QNB would diffuse only along the muscle fibers. No gradient of grain density from the edge of fibers was seen that would suggest QNB diffusion from the muscle fibers into other regions of the preparation.

Comparison to Focal Synapses

The diffuse pattern of innervation and the widespread distribution of mAChR on cardiac muscle fibers is ideally suited for the role the parasympathetic nervous system plays in modulating heart rate. The arrangement of the axonal varicosities suggests that ACh is, in effect, "bath applied" to the muscle. Some indirect evidence for this comes from the observation that several vagal impulses can produce a 20–30 mV hyperpolarization, whereas focal application of ACh from a micropipet produces responses whose peaks saturate quickly with ACh dose (Fig. 5) and are not more than 5–10 mV in amplitude. This suggests that nerve-released transmitter acts at a much lower concentration over a larger area of the muscle membrane than iontophoretically-applied ACh does.

ACh has been shown to modulate the slow, inward Ca^{+2}/Na^+ current of the cardiac action potential (15, 31, 53). The channels of the slow, inward current presumably are distributed throughout the muscle membrane. For ACh to modulate these channels, each channel may be associated directly with a receptor or, alternatively, receptors might affect distant channels by "second messengers" that are formed as the result of ACh-receptor interaction and that diffuse throughout the cell (14, 41). The widespread distribution of ACh receptors in the membrane makes it likely that each channel is associated with a receptor and reduces the need to hypothesize the involvement of second messengers.

The mode of action of ACh in the heart contrasts strongly with that which has been described at "focal" synapses such as the skeletal muscle-nerve junction. At the motor endplate, ACh evokes a fast excitatory postsynaptic potential (epsp) that triggers muscle contraction. The epsp rises to a peak in <1 ms and lasts no more than 50 ms. This fast action of ACh is well adapted to triggering quick muscle twitches at high frequencies. The structure of the neuromuscular junction is highly specialized for providing such rapid action of ACh. The pre- and postsynaptic membranes are closely apposed with a synaptic cleft not exceeding 50 nm. Quanta of ACh are released at discrete spots from the nerve terminal in such a way that each quantum usually affects very small, nonoverlapping areas of postsynaptic membrane (M. M. Salpeter, personal communication; see also reference 24 and footnote 1). The punctate action of ACh is produced in part by the action of the enzyme acetylcholinesterase, which is concentrated in the synaptic region and limits lateral diffusion of ACh and multiple binding (24, 32). Receptors for ACh are highly localized in the subsynaptic membrane: the ACh-receptor packing density in the subsynaptic membrane is $\sim 10^3 \times$ higher than in extrasynaptic membrane several micrometers away (9, 10, 33). This assures that diffusion of ACh from the receptive membrane will occur quickly.

Chemosensitivity of the Receptive Membrane

The ACh sensitivity of cardiac muscle is ~100-fold lower than that found at the skeletal neuromuscular junction (up to 5,000 mV/nC), when sensitivity is expressed in terms of the peak response. The difference in sensitivity of cardiac and skeletal muscle is, in part, a result of a lower receptor density in cardiac compared to skeletal muscle. Autoradiographic experiments in this paper suggest that the heart has a lower receptor density than the endplate. I typically find 0.07 grains/μm^2 with 14 d exposure of autoradiograph. If one assumes that the probability a disintegration will produce a silver grain is 0.25, the mAChR packing density in these preparations is ~130 mAChR/μm^2. This is about two orders of magnitude less than that found at the endplate, but is comparable to that seen in extrajunctional regions of denervated skeletal muscle (8, 22). Receptor density alone, however, does not completely explain the differences in chemosensitivity of cardiac and skeletal muscle, because the ACh sensitivities of cardiac and skeletal muscle are similar when expressed in terms of the time integral

[1] Matthews-Bellinger, J., and M. M. Salpeter. 1978. Distribution of acetylcholine receptors at frog neuromuscular junction with a discussion of some physiological implications. *J. Physiol. (Lond.)*. 279:197–213.

of the response (33 mV·s per nanocoulomb for heart in Fig. 5 and, for example, 17 mV·s per nanocoulomb for endplate from Fig. 4 of reference 33). These results may be explained by recent results by Noma and collaborators (42–44). They have shown that the single-channel conductance of the ACh-activated potassium channels in mammalian SA node is about one-fifth to one-tenth that of the endplate channel but the single-channel lifetime is ~100 × longer than that of the endplate channel. Thus, a given dose of ACh may open fewer channels in heart, but each channel may pass 10–20 × more charge per opening than the endplate channel.

Kinetics of ACh Response

When ACh is iontophoretically applied to a cardiac muscle fiber that is not spontaneously beating, a hyperpolarization is produced that begins with a latency of ~100 ms, reaches a peak in 1–2 s, and decays in an additional several seconds (Fig. 4; see also references 5, 16, 23, 27, 48, 50). Such slowness seems to be a common feature of muscarinic ACh responses in a variety of systems (autonomic neurons, 23, 35; smooth muscle, 4, 49; pancreatic acinar cells, 47). The slow time-course of the response could be explained by diffusional limitations or by cellular mechanisms. For example, the onset of the response might be the result of diffusional barriers restricting ACh access to receptors, and the decay might be caused by repeated ACh receptor binding and slowed ACh diffusion from the receptive membrane. Hill-Smith and Purves (27) have argued effectively that diffusional barriers cannot easily explain the latency or slow onset of the response. The finding (Fig. 16) that ACh receptors are widely distributed over the muscle surface and not restricted to inaccessible clefts further reduces the likelihood of diffusional limitations producing the latency. In addition, the high temperature-sensitivity of the response illustrated in Fig. 6, which is similar to a more extensive analysis by Pott (48), is inconsistent with a simple diffusional mechanism. The initial rising phase of the ACh response can be described by a third-order exponential: $(1 - e^{-\alpha t})^3$ where α is a constant and t is time. α has a Q_{10} of 2.3, so the overall rising phase has a Q_{10} of 12 ($[2.3]^3 = 12.2$).

Diffusional limitations can theoretically predict the declining phase of the ACh response (27). Because ACh receptors are distributed over the entire surface of the muscle, the slow time-course of the response might be explained by diffusion of ACh along the receptive membrane and repeated binding of ACh to its receptors. Additional experiments, however, are required to distinguish between rebinding and the involvement of chemical intermediates (such as cyclic nucleotides) as intracellular effectors of the ACh response (14, 41).

Thanks to Amy Ard, for her delightful and insightful comments, to Vicki Shadix for preparing the manuscript, and to Nola Walker for EM assistance. QNB and tropicamide were gifts from Hoffmann-La Roche. I also thank the reviewers for their very valuable comments.

This study was supported by National Institutes of Health grant HL21195 and Research Career Development Award HL00435.

Received for publication 2 August 1979, and in revised form 30 January 1980.

REFERENCES

1. Abraham, A. 1969. Microscopic Innervation of the Heart and Blood Vessels in Vertebrates Including Man. Oxford University Press, Oxford, England.
2. Akert, K., and C. Sandri. 1975. Significance of the Maillet method for cytochemical studies of synapses. *In* Golgi Centennial Symposium Proceedings. M. Santini, editor. Raven Press, New York.
3. Anderson, M., and J. del Castillo. 1972. Cardiac innervation and synaptic transmission in the heart. *In* Electrical Phenomena in the Heart. M. C. de Mello, editor. Academic Press, In., New York.
4. Bennett, M. R. 1972. *Autonomic Neuromuscular Transmission.* Cambridge University Press, Cambridge, England.
5. Brown, G. L., and J. C. Eccles. 1934. The action of a single vagal volley on the rhythm of the heart beat. *J. Physiol. (Lond.).* 82:211–241.
6. Brown, W. E., and A. V. Hill. 1922. The oxygen-dissociation curve of blood and its thermodynamical basis. *Proc. R. Soc. Lond. B Biol. Sci.* 94:297–334.
7. Cavey, D., J. P. Vincent, and M. Lazdunski. 1977. The muscarinic receptor of heart cell membranes. *FEBS (Fed. Eur. Biochem. Soc.) Lett.* 84:110–114.
8. Fambrough, D. M. 1974. Acetylcholine receptors: Revised estimate of extrajunctional receptor density in denervated rat diaphragm. *J. Physiol. (Lond.).* 64:465–472.
9. Fambrough, D. M., and H. C. Hartzell. 1972. Acetylcholine receptors: Number and distribution at neuromuscular junctions in rat diaphragm. *Science (Wash. D. C.).* 176:189–191.
10. Fertuck, H. C., and M. M. Salpeter. 1976. Quantitation of junctional and extrajunctional acetylcholine receptors by electron microscope autoradiography after ^{125}I-α-bungarotoxin binding at mouse neuromuscular junctions. *J. Cell Biol.* 69:144–158.
11. Fields, J. Z., W. R. Roeske, E. Morkin, and H. I. Yamamura. 1978. Cardiac muscarinic cholinergic receptors. *J. Biol. Chem.* 253:3251–3258.
12. Galper, J. B., W. Klein, and W. A. Catterall. 1977. Muscarinic acetylcholine receptors in developing chick heart. *J. Biol. Chem.* 252:8692–8699.
13. Garnier, D., J. Nargeot, C. Ojeda, and O. Rougier. 1978. The action of acetylcholine on background conductance in frog atrial trabeculae. *J. Physiol. (Lond.).* 274:381–396.
14. George, W. J., J. B. Polson, A. G. O'Toole, and N. D. Goldberg. 1970. Elevation of guanosine 3',5' cyclic phosphate in rate heart after perfusion with acetylcholine. *Proc. Natl. Acad. Sci. U. S. A.* 66:398–403.
15. Giles, W., and S. J. Noble. 1976. Changes in membrane currents in bullfrog atrium produced by acetylcholine. *J. Physiol. (Lond.).* 261:103–123.
16. Glitsch, H. G., and L. Pott. 1978. Effects of acetylcholine and parasympathetic nerve stimulation on membrane potential in quiescent guinea pig atria. *J. Physiol. (Lond.).* 279: 655–668.
17. Grillo, M. A. 1966. Electron microscopy of sympathetic tissues. *Pharmacol. Rev.* 18:387 399.
18. Hadek, R., and P. J. Talso. 1967. A study of nonmyelinated nerves in the rat and rabbit heart. *J. Ultrastruct. Res.* 17:257–265.
19. Harris, A. J., S. W. Kuffler, and M. J. Dennis. 1971. Differential chemosensitivity of synaptic and extrasynaptic areas on the neuronal surface membrane in parasympathetic neurons of the frog, tested by microapplication of acetylcholine. *Proc. R. Soc. Lond. B Biol. Sci.* 177:541–553.
20. Hartzell, H. C. 1979. Adenosine receptors in frog sinus venosus: Slow inhibitory potentials produced by adenine compounds and acetylcholine. *J. Physiol. (Lond.).* 293:23–49.
21. Hartzell, H. C. 1979. Distribution of muscarinic acetylcholine receptors in amphibian cardiac muscle. *Nature (Lond.).* 278:569–571.
22. Hartzell, H. C., and D. M. Fambrough. 1972. Acetylcholine receptors: Distribution and extrajunctional density in rat diaphragm after denervation correlated with acetylcholine sensitivity. *J. Gen. Physiol.* 60:248–262.
23. Hartzell, H. C., S. W. Kuffler, R. Stickgold, and D. Yoshikami. 1977. Synaptic excitation and inhibition resulting from direct action of acetylcholine on two types of chemoreceptors on individual amphibian parasympathetic neurones. *J. Physiol. (Lond.).* 271:817–846.
24. Hartzell, H. C., S. W. Kuffler, and D. Yoshikami. 1975. Post-synaptic potentiation: Interaction between quanta of acetylcholine at the skeletal neuromuscular synapse. *J. Physiol. (Lond.).* 251:427–463.
25. Higgins, C. B., S. F. Vatner, and E. Braunwald. 1973. Parasympathetic control of the heart. *Pharmacol. Rev.* 25:119–155.
26. Hillarp, N.-A. 1959. The construction and functional organization of the autonomic innervation apparatus. *Acta. Physiol. Scand.* (Suppl. 157) 46:1–38.
27. Hill-Smith, I., and R. D. Purves. 1978. Synaptic delay in the heart: An iontophoretic study. *J. Physiol. (Lond.).* 279:31–54.
28. Hirsch, E. F. 1970. Innervation of the Vertebrate Heart. Charles C. Thomas, Publisher. Springfield, Ill.
29. Hoffman, B. F., and P. F. Cranefield. 1960. Electrophysiology of the Heart. McGraw-Hill, Inc., New York.
30. Hollenberg, M. D., and P. Cuatrecassas. 1976. Membrane receptors and hormone action. *Adv. Protein Chem.* 30:251–451.
31. Ikemoto, Y., and M. Goto. 1975. Nature of the negative inotropic effect of acetylcholine on the myocardium. An elucidation on the bullfrog atrium. *Proc. Jpn. Acad.* 51:501–505.
32. Katz, B., and R. Miledi. 1973. The binding of acetylcholine to receptors and its removal from the synaptic cleft. *J. Physiol. (Lond.).* 231:549–574.
33. Kuffler, S. W., and D. Yoshikami. 1975. The distribution of acetylcholine sensitivity at the post-synaptic membrane of vertebrate skeletal twitch muscles. Iontrophoretic mapping in the micron range. *J. Physiol. (Lond.).* 244:703–730.
34. Lane, M., A. Sastre, M. Law, and M. M. Salpeter. 1977. Cholinergic and adrenergic receptors on mouse cardiocytes in vitro. *Dev. Biol.* 57:254–269.
35. Libet, B. 1970. Generation of slow inhibitory and excitatory post-synaptic potentials. *Fed. Proc.* 29:1945–1956.
36. Maekawa, M., Y. Nohara, K. Kawamura, and K. Hayashi. 1967. Electron microscope study of the conduction system in mammalian hearts. *In* Electrophysiology and Ultrastructure of the Heart. T. Sano, V. Mizuhira, and K. Matsuda, editors. Grune & Stratton, Inc., New York. 41–54.
37. Maillet, M. 1962. La technique de Champy à l'osmium ioduré de potassium et la modification de Maillet à l'osmium ioduré de zinc. *Trab. Inst. Cajal Invest. Biol.* 54:1–36.
38. Marshall, J. M. 1974. The heart. *In* Medical Physiology. Vol. 2. 13th ed. V. B. Mountcastle, editor. C. V. Mosby Co. St. Louis. 849–882.
39. McMahan, U. J., and S. W. Kuffler. 1971. Visual identification of synaptic boutons on living ganglion cells and of varicosities in postganglionic axons in the heart of the frog. *Proc. R. Soc. Lond. B Biol. Sci.* 177:485–508.
40. Miledi, R. 1960. The acetylcholine sensitivity of frog muscle fibers after complete or partial denervation. *J. Physiol. (Lond.).* 151:1–23.
41. Nawrath, H. 1977. Does cyclic GMP mediate the negative inotropic effect of acetylcholine in the heart? *Nature (Lond.).* 267:72–74.
42. Noma, A., W. Osterrieder, and W. Trautwein. 1979. The effect of external potassium on the elementary conductance of the ACh-induced potassium channel in the sino-atrial node. *Pfluegers Arch. Eur. J. Physiol.* 381:263–269.
43. Noma, A., K. Peper, and W. Trautwein. 1979. Acetylcholine induced potassium current

fluctuations in rabbit sino-atrial node. *Pfluegers Arch. Eur. J. Physiol.* 381:255–262.
44. Noma, A., and W. Trautwein. 1978. Relaxation of the ACh-induced potassium current in the rabbit sinoatrial node cell. *Pfluegers Arch. Eur. J. Physiol.* 377:193–200.
45. Novi, A. M. 1968. An electron microscopic study of the innervation of papillary muscles in the rat. *Anat. Rec.* 160:123–142.
46. Pellegrino de Iraldi, A. 1977. Significance of the Maillet method (ZIO) for cytochemical studies of subcellular structures. *Experientia (Basel).* 33:1–34.
47. Peterson, O. H. 1976. Electrophysiology of mammalian gland cells. *Physiol. Rev.* 56:535–577.
48. Pott, L. 1979. On the time course of the acetylcholine-induced hyperpolarization in quiescent guinea pig atria. *Pfluegers Arch. Eur. J. Physiol.* 380:71–77.
49. Purves, R. D. 1974. Muscarinic excitation: A microelectrophoretic study on cultured smooth muscle cells. *Br. J. Pharmacol.* 52:77–86.
50. Purves, R. D. 1976. Function of muscarinic and nicotinic acetylcholine receptors. *Nature (Lond.).* 261:149–151.
51. Roper, S. 1976. The acetylcholine sensitivity of the surface membrane of multiply-innervated parasympathetic ganglion cells in the mudpuppy before and after partial denervation. *J. Physiol. (Lond.).* 254:455–473.
52. Scatchard, G. 1949. The attractions of proteins for small molecules and ions. *Ann. N. Y. Acad. Sci.* 51:660–672.
53. Ten Eick, R., H. Nawrath, T. F. McDonald, and W. Trautwein. 1976. On the mechanism of the negative inotropic effect of acetylcholine. *Pfluegers Arch. Eur. J. Physiol.* 361:207–213.
54. Thaemert, J. C. 1969. Ultrastructure of cardiac muscle and nerve contiguities. *J. Cell Biol.* 29:156–162.
55. Thaemert, J. C. 1970. Atrioventricular node innervation in ultrastructural three dimensions. *Am. J. Anat.* 128:239–264.
56. Trautwein, W., and K. Uchizono. 1963. Electron microscopic and electrophysiologic study of the pacemaker in the sino-atrial node of the rabbit heart. *Z. Zellforsch. Mikrosk. Anat.* 61:96–109.
57. Woods, R. I. 1970. The innervation of the frog's heart. I. An examination of the autonomic postganglionic nerve fibers and a comparison of autonomic and sensory ganglion cells. *Proc. R. Soc. Lond. B Biol. Sci.* 176:43–54.
58. Woods, R. I. 1970. The innervation of the frog's heart. III. Electron microscopy of the autonomic nerve fibers and their vesicles. *Proc. R. Soc. Lond. B Biol. Sci.* 176:63–68.
59. Yamamura, H. I., and S. H. Snyder. 1974. Muscarinic cholinergic receptor binding in the longitudinal muscle of the guinea pig ileum with ^{3}H-quinuclidinyl benzilate. *Mol. Pharmacol.* 10:861–867.